SCIENCE CHINA
Information Sciences

• RESEARCH PAPER •

September 2022, Vol. 65 192301:1–192301:14
https://doi.org/10.1007/s11432-020-3202-2

Enhanced time-expanded graph for space information network modeling

Jiandong LI, Peng WANG*, Hongyan LI & Keyi SHI

State Key Laboratory of Integrated Service Networks, Xidian University, Xi'an 710071*, China*

Received 7 September 2020/Revised 9 December 2020/Accepted 5 March 2021/Published online 25 August 2022

Abstract Space information networks (SINs) are responsible for communications, information processing, and earth observation. Traditional time-expanded graphs (TEG) cannot represent the observation, energy, and transceiver resources. Therefore, we propose the enhanced time-expanded graph (ETEG) to jointly model the resource elements of SINs. First, we utilize snapshot graphs to characterize the time-varying properties of the resources. Next, we introduce virtual links and nodes to enhance the TEG, which transforms the transceiver and observation resource constraints into normal capacity and flow conservation ones and simplifies the energy constraints. Then, the maximum flow algorithm is modified to optimally schedule the data flow in SIN. With the ETEG-based maximum flow algorithm, the resources can be jointly optimally scheduled. Finally, the simulation results demonstrate the efficiency and effectiveness of our ETEG.

Keywords enhanced time-expanded graph, space information network, network modeling, heterogeneous resource modeling, joint scheduling

Citation Li J D, Wang P, Li H Y, et al. Enhanced time-expanded graph for space information network modeling. Sci China Inf Sci, 2022, 65(9): 192301, https://doi.org/10.1007/s11432-020-3202-2

1 Introduction

Space information networks (SINs) possess wide coverage and flexible networking [1]. Particularly, they can provide continuous services, i.e., earth observation, meteorology, environment and disaster monitoring, resource survey, topographic mapping and ocean-going voyage communication [2–4].

Owing to the inherent mobility of satellites, SINs are characterized by time-varying topology with heterogeneous resources, e.g., transceiver, caching, observation, and energy resources. In fact, transceiver resources contain transmitter and receiver resources, which determine the total transmission ability (i.e., the data amount one satellite can transmit within a time period) and reception ability (i.e., the amount of data a satellite can receive over a period of time) for one satellite. Besides, onboard memories are the caching resources of satellites, which are used to store a limited amount of data. Furthermore, observation resources refer to onboard imaging sensors (e.g., optical cameras), which provide a limited information acquisition rate. Finally, energy is generated by the Solar panels of satellites, to support data transmission and other daily operations (e.g., rotate sensors, store data) for satellites.

Precisely and efficiently modeling the time-varying topology and resources for SINs is the basis for optimum resource scheduling, which faces the following challenges. (1) How to model the time-varying topology for SINs, so that the scarce transmission opportunities distributed in space and time dimensions can be jointly utilized. (2) How to jointly model the heterogeneous resources for SINs, so that the coordination among resources can be supported. For instance, as shown in Figure 1(a), we consider a simple network in two time slots and the length of each time slot is 1 s. Besides, it contains links (S, A) and (A, D) with transmission rates of 50 and 20 Mbps in the first slot, respectively. And the rates for (S, A) and (A, D) in the second slot are 20 and 50 Mbps, respectively. Then, as shown in Figure 1(b), if the caching resources of A do not cooperate with link resources, only 20 Mb can be transmitted from S to D in each time slot, and an average rate of only 20 Mbps can be reached. However, resorting to

* Corresponding author (email: pengwangclz@163.com)

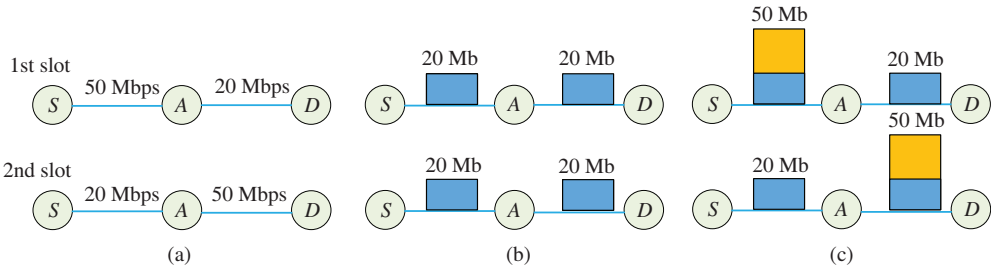

Figure 1 (Color online) The effect of resource cooperation on network performance. (a) Network topology. End-to-end transmission without (b) and with (c) resource cooperation.

Figure 1(c), in the first slot, S transmits 50 Mb of data to A, and A stores 30 Mb of data and transmits 20 Mb to D. Then in the second slot, 20 Mb of data is transmitted to A, then A transmits its received and stored data, which reaches 50 Mb, to D. Hence, 70 Mb of data is transmitted to D over 2 time slots and an average rate of 35 Mbps is achieved. Thus, it follows that the storage resources can combine and bridge the scarcely distributed link resources and the cooperation between multiple resources can significantly improve the network performance[1)].

There have been extensive network modeling-related works. In the existing terrestrial network modeling methods, e.g., [5, 6], SINs are treated as static networks and the cooperation between caching and link resources is ignored, resulting in low network resource utilization. As for the time-varying network modeling methods, they can be roughly categorized as mathematical programming methods and graph-based methods.

For the mathematical programming methods, Refs. [7, 8] considered the caching, transponder, and energy resources constraints to deal with the capacity analysis and mission-aware contact plan design problems, respectively. In [7,8], the time-expanded graphs were constructed only to illustrate the solution space because no graph-based algorithms were involved and both problems were solved as mixed integer linear programming (MILP) ones. In addition, Wang et al. [9] considered the transceiver, buffer and observation resource constraints for SIN, and then modeled the observation scheduling problem as one integer linear programming (ILP) problem, without involving the energy constraints. The aforementioned linear programming could better model complex resource constraints, yet with higher time complexity compared to the graph-based methods.

For the second category, the authors in [10] designed one optimum snapshot division strategy to improve the network performance. Besides, time-expanded graph (TEG) and graph-based algorithms were modified and designed to solve multi-cast [11], resource allocation [12], and capacity analysis [13] problems for the network, respectively. Furthermore, George et al. [14] aggregated the information of each snapshot into series and constructed the time aggregated graph (TAG), which could improve the computation efficiency compared to the TEG. However, the storage resources were not involved in [14] in the TAG. As a result, one storage time aggregated graph (STAG) was proposed in [15] to jointly model the link and storage resources. Furthermore, STAG was also utilized to construct QoS-guaranteed routing [16] and maximum two-commodity flow [17]. Moreover, Jiang et al. [18] proposed the concept of temporal centrality and achieved load balance in SIN. Although these graph-based methods are efficient, only the modeling for link and caching resources were addressed. Particularly, the physical problem, namely, the jointly scheduling of heterogeneous resources including energy and transceiver resources, is unresolved.

To further illustrate the difference between these two categories, we compare the two categories in the same problem, indicating that the time complexity of linear programming is higher than that of the graph based modeling method. For instance, when solving the maximum flow problem with n nodes and m edges, the time complexity for the linear programming (LP) [8] reaches $O(m^{3.5})$, while the graph-based Edmond-Karp algorithm [19] is $O(n^2m)$. To be more specific, in two strongly-connected networks with 1000 and 2000 nodes, the graph based-methods outperform the linear-programming methods in terms of the running time as shown in Figure 2.

The problem of scheduling caching, transceiver, observation, and energy resources are unresolved to our best knowledge. To overcome the problem efficiently, we enhance the ability of the graph to model

1) Note that, caching resources only involve in when congestion occurs in traditional routing strategy, we are suggesting a different modeling method and utilization strategy for heterogeneous resources including caching resources and link resources.

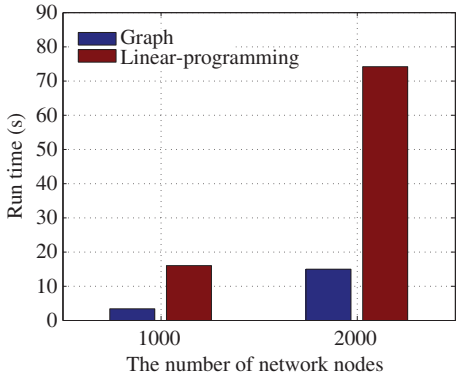

Figure 2 (Color online) The running time for LP and Edmond-karp algorithms when solving the maximum flow algorithm.

SIN and propose an enhanced time-expanded graph (ETEG), which jointly depicts different resources in SIN. Then, the maximum flow algorithm is modified via introducing two computation rules to further guarantee feasible resource scheduling. Specifically, our contributions are listed as follows:

• To guarantee the feasibilities and accuracy of modeling, the characteristics and the resource elements affecting the information transmission of SIN are analyzed. Then the necessity for jointly modeling is given.

• To take full advantage of graph theory, we propose a method to construct the ETEG so that different kinds of resources and time-varying topology can be uniformly characterized as links and quantified as weights on links. As such, the special constraints of resources are transformed into traditional capacity constraints and flow conservation via introducing virtual nodes and links.

• In order to optimize the utilization of resources, we modify the traditional maximum flow algorithm and propose two kinds of computation rules to achieve the maximum capacity of end-to-end transmission, which also achieves joint scheduling of different resources. Then the ETEG-based method outperforms the independent scheduling (i.e., independent transmission and observation) method and independent resource allocation methods in terms of network throughput. Hence, our proposed ETEG effectively combines the transmission and observation phases and enables the cooperation between resources.

2 Characteristics of space information networks

SIN is responsible for data acquisition, processing, and transmission. As shown in Figure 3, similar to [1,3], we consider a satellite architecture, which includes (i) deep space spacecrafts conducting Lunar/Mars and other deep space missions, (ii) geostationary satellites made up of backbone networks and providing global communications, (iii) near earth orbits spacecrafts performing earth observation and space experiment tasks, (iv) near space planes and UAVs, and (v) terrestrial networks. Furthermore, we consider earth observation and communication missions in SIN. Earth observation missions refer to that satellites use their imaging sensors to observe target areas on ground and obtain observed data, and the communication missions are that the satellites transmit their data to ground stations with the help of other satellites while satisfying the delay requirements of data. And SINs have the following characteristics,

• **Heterogeneity of resources.** In fact, relationships among the resources are complicated as shown in Figure 4. For instance, the limited electronic energy generated by the Solar panels will power and limit the use of transceiver, caching, and observation resources. Besides, the caching resources can bridge sparsely distributed transmission resources to generate an end-to-end path across time from satellites to ground stations. Likewise, observation resources distributed across time can also be bridged by caching resources to finish one observation mission. Furthermore, as the data generated by observation missions will be the input of communication missions, the available transmission ability will affect the observation decisions. To be more specific, let observation satellites 1 and 2 be able to observe one same target at the same time. After observation, suppose observation satellite 1 can transmit the observed data to ground stations in a multi-hop manner and meet the delay requirement while satellite 2 cannot meet the requirement, then, it is better to choose satellite 1 to observe the mission. Thus, the available transceiver resources will affect and limit the use of observation resources.

• **Time-varying topology.** Due to the mobility of satellites, the communication links between

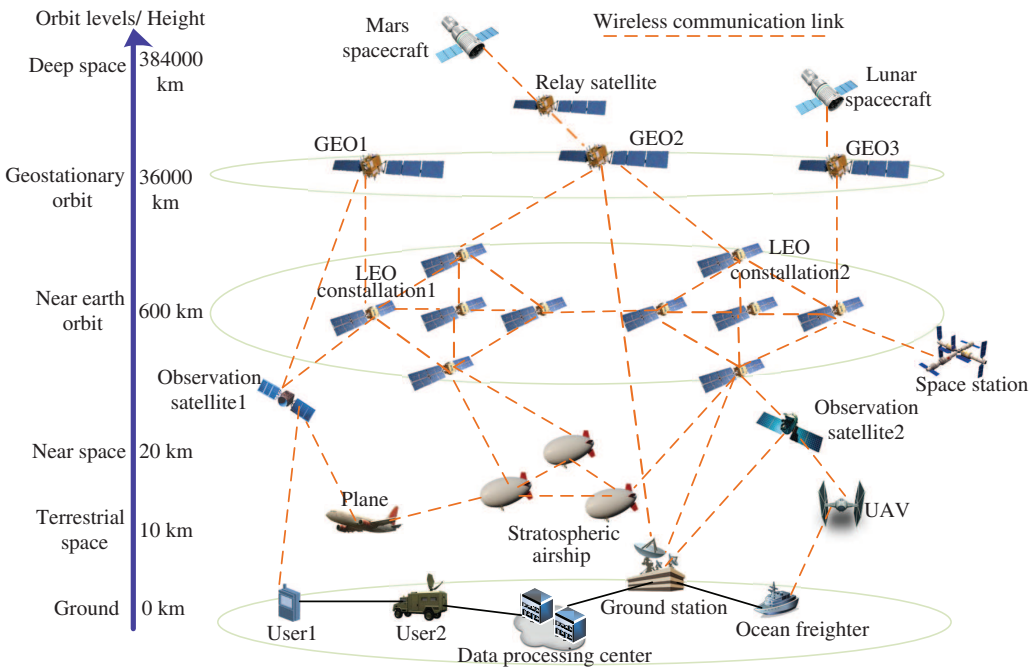

Figure 3 (Color online) Architecture of space information networks.

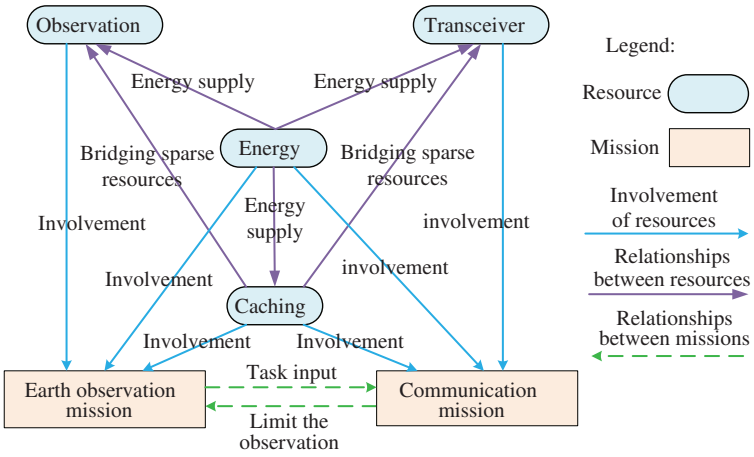

Figure 4 (Color online) The relationships among resources and missions.

satellites can be established only when they fly into the communication range of each other, and the links become disconnected when they fly out [1]. Thus, the mobility of satellites results in a time-varying topology for SIN. Due to the sparse distribution of resources, resources across time need to be bridged to finish the observation and communication missions, which relies on accurate modeling of time-varying topology.

• **Low resource utilization by independent scheduling.** In fact, the observation and communication missions are usually independently scheduled as in [8, 16, 20]. That is, the observation missions scheduling only focuses on how to maximize the observation [20], while the communication missions mainly focus on maximizing the end-to-end transmission [16]. Then, for observed data that has tight delay requirements, it is possible the data cannot be transmitted to the ground stations with its delay guaranteed, because the transmission capacity from this observation satellite to ground station is small before the deadline. Hence, to support joint scheduling, it is necessary to jointly represent the observation and communication missions in one graph.

As a result, to model SIN, the relationships in Figure 4 and the time-varying topology of SIN should be incorporated.

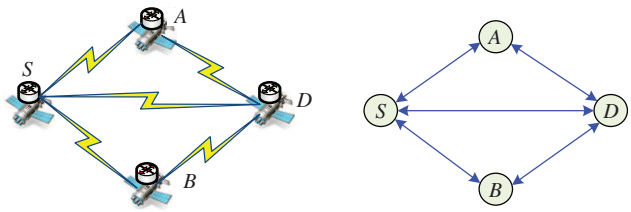

(a) (b)

Figure 5 (Color online) An example of traditional graph representation. (a) An example of network topology; (b) traditional graph representation.

3 Enhanced time-expanded graph construction

To enhance the ability to model networks for graphs, in this section, the features of traditional graphs are first analyzed. Then, we propose an ETEG to model the resource elements of SIN. Finally, computation rules are designed to model the energy and transceiver resources consumption process.

3.1 Characteristics of traditional graph

As shown in Figure 5, consider graph $G = (V, E)$ that consists of node set V and edge set E. V depicts the entities of communication networks, while edge set E represents the communication links between nodes. For instance, graph model for network in Figure 5(a) is shown in Figure 5(b).

Furthermore, let the maximum amount of data that u can transmit to v (i.e., the capacity of (u, v)) and the amount of data flowing through link $(u, v) \in E$ be $C_{u,v}$ and $f_{u,v}$, respectively. Suppose S and D are the source and destination nodes in G, and G involves two constraints:

Capacity constraints on link. The flow goes through any link cannot exceed its maximum transmission ability, namely,

$$f_{u,v} \leqslant C_{u,v}, \quad \forall (u, v) \in E. \tag{1}$$

Flow conservation on node[2)]**.** The amount of flow into any node of V except S and D should be equal to that out of the node, namely,

$$\sum_{u \in V} f_{u,v} = \sum_{u \in V} f_{v,u}, \quad \forall v \in V - \{S, D\}. \tag{2}$$

With the two constraints, with traditional graph $G = (V, E)$, maximum flow, shortest path and minimum cost flow from S to D can be identified with well investigated network flow algorithms [19,21]. Furthermore, these optimum flow requires optimum scheduling of resources. Thus, these algorithms [19,21] can be utilized to achieve optimal resource scheduling of network.

3.2 SIN elements modeling

Traditional graph cannot model SINs as the resources of SINs introduce constraints different from (1) and (2). As a result, to take full advantage of graph theory, the modeling capacity of traditional graph needs to be enhanced.

To obtain the enhanced time-expanded graph, we first model SIN's time-varying topology. Then the different types of resources are modeled one by one. For clearness, one simplified example topology derived from Figure 3 is presented in Figure 6(a). Particularly, the SIN contains mission set $\mathcal{M} = \{\mathbb{M}_1, \mathbb{M}_2\}$ where $\mathbb{M}_1$ and $\mathbb{M}_2$ represents missions 1 and 2, one observation satellite $\mathbb{O}_1$, 3 low Earth orbit (LEO) satellites $\mathbb{L}_1$, $\mathbb{L}_2$, $\mathbb{L}_3$, and one ground station $\mathbb{G}$. Furthermore, the opportunity time windows along time horizon T for the communications and observations are shown in Figure 6(b).

(a) Time-varying topology modeling. As the satellites flight trajectories are predictable, for the network in Figure 6(a), we can obtain the connection time windows for any two entities (i.e., satellite, observation mission, and ground station) in the network in time horizon T. For instance, in Figure 6(b), the observation time windows between $\mathbb{M}_1$ and $\mathbb{O}_1$ (i.e., M_1-O_1 in Figure 6(b)) lie in time periods $[t_1, t_2]$ and $[t_3, t_4]$, while the communication time window for $\mathbb{L}_1$ and $\mathbb{O}_1$ (i.e., L_1-O_1) lies in $[t_2, t_3]$. Then we

2) In fact, flow conservation are requirements for perfect scheduling and no loss of data at nodes rather than constraints. For convenient illustration, we call it as constraint.

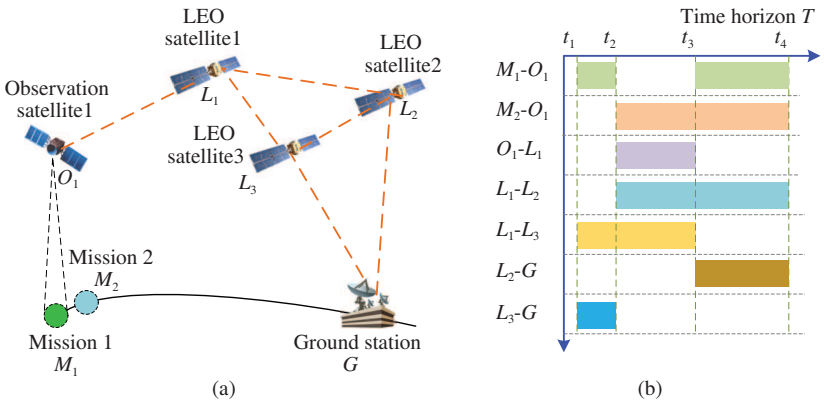

Figure 6 (Color online) (a) A simple network of SIN; (b) time windows of connections in the network along time horizon T.

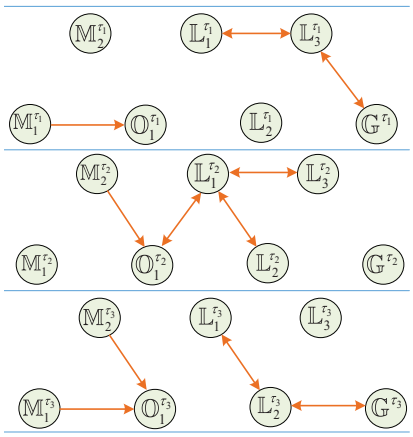

Figure 7 (Color online) Time-varying topology of SIN.

sort all the start and end times in descending order for all the time windows of all the observation and communication time windows, and obtain $\{t_1, t_2, t_3, t_4\}$. In the list, each two adjacent time elements are the start and end times of one snapshot. And note that the snapshot depicts the SIN topology of one time period. As such, all the evolving topologies of the SIN in T can be recorded as snapshots.

Similar to [10], after determining the time period (i.e., start and end times) of each snapshot, the time-varying topology can be obtained as shown in Figure 7. The topology includes,

• $T = [t_1, t_h) = \{\tau_1, \ldots, \tau_{h-1}\}$, the time horizon, is constructed with small time slots. In particular, τ_p is defined as the time period of the p_{th} snapshot and $\tau_p = [t_p, t_{p+1})$. Besides, we let $|\tau_p| = t_{p+1} - t_p$ to represent the length of the p_{th} time period. For instance, in Figure 6, we will have $T = [t_1, t_4) = \{\tau_1, \tau_2, \tau_3\}$, where $\tau_2 = [t_2, t_3)$. Furthermore, as satellites will harvest and consume electricity while orbiting earth, we consider T as a time period for satellites to consume energy.

• $\mathcal{V}$: the set of nodes, consists of the replicas of given satellites, ground stations and missions in each time slot. For any entity u within time slot τ_p, we denote it as u^{τ_p}.

• $\mathcal{E}$: the set of edges, includes directional and bidirectional edges. Specifically, the former ones represent observation opportunities when targets are within observation range of satellites, while the latter ones characterize the communication opportunities when two satellites (or one satellite and one ground station) can communicate with each other. Besides, we use $(\cdot)$ and $[\cdot]$ to depict directional and bidirectional edges, respectively.

• $\mathcal{W}$: the weight of edges with unit Gb. For any edge $e \in \mathcal{E}$, its weight is W_e, which refers to the maximum data amount that can be transmitted or observed through e. Particularly, the weight for any observation link between satellite u and mission $\mathbb{M}_i$ in τ_p is denoted as $W^{\tau_p}_{u,\mathbb{M}_i}$, which equals the data volume $v(\mathbb{M}_i)$ of $\mathbb{M}_i$. Specifically, the unit of $v(\mathbb{M}_i)$ is Gb. Then for bidirectional link $[u, v]$ in τ_p, we use $W^{\tau_p}_{u,v}$ and $W^{\tau_p}_{v,u}$ to represent the maximum data amount of u can transmit to v and of v to u, respectively. Particularly, let the transmission rate of (u, v) and (v, u) in τ_p be $R^{\tau_p}_{u,v}$ and $R^{\tau_p}_{v,u}$, respectively. Then, $W^{\tau_p}_{u,v} = R^{\tau_p}_{u,v} \times |\tau_p|$ while $W^{\tau_p}_{v,u} = R^{\tau_p}_{v,u} \times |\tau_p|$.

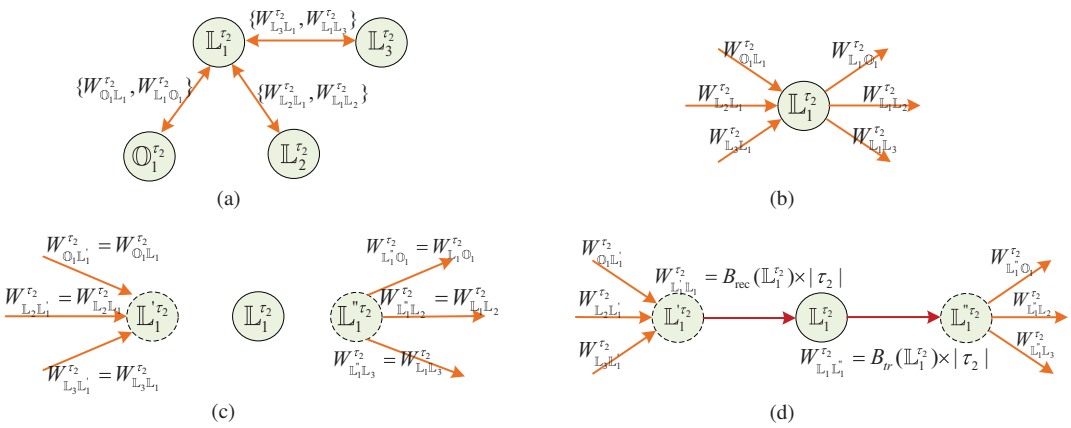

Figure 8 (Color online) Graph operations for transceiver constraint relation representation. (a) Original topology; (b) step 1; (c) step 2; (d) step 3.

• f: the decision variable, is the determined amount of flow through edges. For any link $(u, v) \in \mathcal{E}$, the determined flow through it in τ_p is $f_{u,v}^{\tau_p}$ with unit as Gb.

(b) Transceiver resource modeling. We assume each satellite carries the phased-array multi-beam antennas as in [22, 23], so that one satellite can communicate with multiple satellites at the same time. Furthermore, the link transmission rate between satellites can be dynamically adjusted, and the handover delay between satellites can be ignored.

For any satellite $\mathbb{L}_i$ in τ_p, let its total transmission and reception rate be $B_{\text{tr}}(\mathbb{L}_i^{\tau_p})$ and $B_{\text{rec}}(\mathbb{L}_i^{\tau_p})$, respectively. Then, the maximum transmission rate for link $(\mathbb{L}_i^{\tau_p}, \mathbb{L}_j^{\tau_p})$ is $R_{\mathbb{L}_i,\mathbb{L}_j}^{\tau_p} = \min\{B_{\text{tr}}(\mathbb{L}_i^{\tau_p}), B_{\text{rec}}(\mathbb{L}_j^{\tau_p})\}$. In fact, link $(\mathbb{L}_i^{\tau_p}, \mathbb{L}_j^{\tau_p})$ achieves its maximum transmission rate if and only if $\mathbb{L}_i^{\tau_p}$ and $\mathbb{L}_j^{\tau_p}$ allocate all of its transmitter resources and receiver resources to the link, respectively. That is, $\mathbb{L}_i^{\tau_p}$ allocates $B_{\text{tr}}(\mathbb{L}_i^{\tau_p})$ to $(\mathbb{L}_i^{\tau_p}, \mathbb{L}_j^{\tau_p})$, while $\mathbb{L}_j^{\tau_p}$ allocates $B_{\text{rec}}(\mathbb{L}_j^{\tau_p})$ to the link.

Then, for any satellite $\mathbb{L}_i$ in τ_p, the sum of its received data from different incoming links cannot exceed the reception ability of its receiver resources, namely,

$$\sum_{\forall \mathbb{A} \in \mathcal{V}} f_{\mathbb{A},\mathbb{L}_i}^{\tau_p} \leqslant B_{\text{rec}}(\mathbb{L}_i^{\tau_p}) \times |\tau_p|. \tag{3}$$

Similarly, all the data transmitted from $\mathbb{L}_i$ in τ_p cannot exceed its transmission ability of transmitters, i.e.,

$$\sum_{\forall \mathbb{A} \in \mathcal{V}} f_{\mathbb{L}_i,\mathbb{A}}^{\tau_p} \leqslant B_{\text{tr}}(\mathbb{L}_i^{\tau_p}) \times |\tau_p|. \tag{4}$$

It is straightforward that the transceiver resource constraints (3) and (4) limit the reception and transmission ability of the nodes, which are different from the traditional link constraints (1) and node constraint (2) in form, making it challenging to satisfy the transceiver resource constraints. However, Eqs. (3) and (4) are similar to (1) in essence because both of them depict the unequal relationships between variables and constant.

Therefore, graph modification is proposed to divide the constraints (3) and (4) into normal flow conservation and capacity constraints similar to [12], and then well investigated maximum flow algorithms can be adopted to satisfy the transceiver constraints. For clearness, the specific transceiver resource modeling process for satellite $\mathbb{L}_1^{\tau_2}$ in Figure 7 is shown in Figure 8.

To characterize the reception constraint (3) for node $\mathbb{L}_1^{\tau_2}$, reception constraint link $(\mathbb{L}_1'^{\tau_2}, \mathbb{L}_1^{\tau_2})$ is introduced in the above representation. Then, due to flow conservation on $\mathbb{L}_1'^{\tau_2}$, the multiple variables in (3) are integrated into one new variable $f_{\mathbb{L}_1',\mathbb{L}_1}^{\tau_2}$. Next, according to capacity constraint (1), we assign $B_{\text{rec}}(\mathbb{L}_1^{\tau_2})$ to the weight of reception constraint link $(\mathbb{L}_1'^{\tau_2}, \mathbb{L}_1^{\tau_2})$. Thus, Eq. (3) is transformed into one flow conservation on $\mathbb{L}_1'^{\tau_2}$ and one capacity constraint on $(\mathbb{L}_1'^{\tau_2}, \mathbb{L}_1^{\tau_2})$, i.e.,

$$\sum_{\forall \mathbb{A} \in \mathcal{V}} f_{\mathbb{A},\mathbb{L}_1}^{\tau_2} = \sum_{\forall \mathbb{A} \in \mathcal{V}} f_{\mathbb{A},\mathbb{L}_1'}^{\tau_2} = f_{\mathbb{L}_1',\mathbb{L}_1}^{\tau_2} \leqslant W_{\mathbb{L}_1',\mathbb{L}_1}^{\tau_2} = B_{\text{rec}}(\mathbb{L}_1^{\tau_2}) \times |\tau_2|. \tag{5}$$

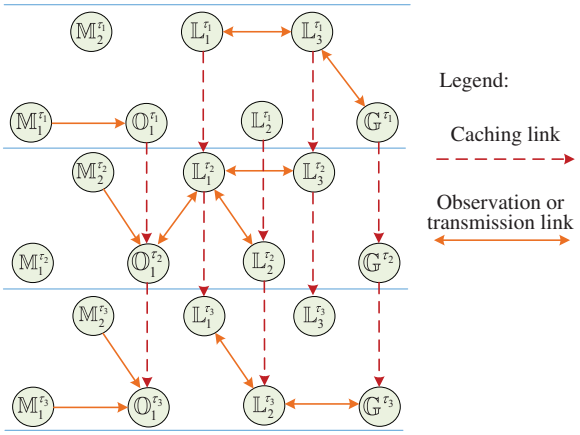

Figure 9 (Color online) Graph operations for caching constraint relation representation (i.e., time-expanded graph).

Similarly, the transmission constraint (4) is also transformed into flow conservation on $\mathbb{L}_1^{\prime\prime\tau_2}$ and capacity constraints on $(\mathbb{L}_1^{\tau_2}, \mathbb{L}_1^{\prime\prime\tau_2})$. Namely,

$$\sum_{\forall \mathbb{A}\in\mathcal{V}} f^{\tau_2}_{\mathbb{L}_1,\mathbb{A}} = \sum_{\forall \mathbb{A}\in\mathcal{V}} f^{\tau_2}_{\mathbb{L}_1'',\mathbb{A}} = f^{\tau_2}_{\mathbb{L}_1,\mathbb{L}_1''} \leqslant W^{\tau_2}_{\mathbb{L}_1,\mathbb{L}_1''} = B_{\mathrm{tr}}(\mathbb{L}_1^{\tau_2}) \times |\tau_2|. \tag{6}$$

(c) Caching resource modeling. Given any relay node u, traditional node constraint (2) requires all the received data of u to be transmitted. However, different from (2), during a time period, u can store part of received data with the help of the caching resources, and transmit the remaining data. In this way, one satellite can store the received data when there is no transmission opportunity, then carry and transmit the stored data until next communication opportunity occurs.

Formally, let available caching size in τ_p for any satellite $\mathbb{L}_i$ be $C^{\tau_p}_{\mathbb{L}_i}$. For the received data of $\mathbb{L}_i$ in τ_p (i.e., $\sum_{\mathbb{A}\in\mathcal{V}} f^{\tau_p}_{\mathbb{A},\mathbb{L}_i}$), some of it will be transmitted (i.e., $\sum_{\mathbb{A}\in\mathcal{V}} f^{\tau_p}_{\mathbb{L}_i,\mathbb{A}}$), while the other data is stored in $\mathbb{L}_i$. And the stored data cannot exceed the caching size. This can be formulated as

$$\sum_{\mathbb{A}\in\mathcal{V}} f^{\tau_p}_{\mathbb{A},\mathbb{L}_i} - \sum_{\mathbb{A}\in\mathcal{V}} f^{\tau_p}_{\mathbb{L}_i,\mathbb{A}} \leqslant C^{\tau_p}_{\mathbb{L}_i}. \tag{7}$$

It is straightforward that the feature of the caching resource cannot be modeled by traditional graph. Fortunately, with new edges inserted as shown in Figure 9, the broken flow conservation can be transformed into normal flow conservation constraints. Specifically, as in [24], new edges are inserted for the same satellite or ground station nodes across two successive time slots. And the capacity of the new edges equals to the available caching size in that time slot. For instance, in Figure 9, new edge $(\mathbb{L}_1^{\tau_1}, \mathbb{L}_1^{\tau_2})$ is inserted with $W_{\mathbb{L}_1^{\tau_1},\mathbb{L}_1^{\tau_2}} = C^{\tau_1}_{\mathbb{L}_1}$.

As such, the constraint relations (7) can be transformed into the traditional flow conservation on node $\mathbb{L}_i^{\tau_p}$ and capacity constraint on edge $(\mathbb{L}_i^{\tau_p}, \mathbb{L}_i^{\tau_{p+1}})$, which is recast as follows:

$$\sum_{\mathbb{A}\in\mathcal{V}} f^{\tau_p}_{\mathbb{A},\mathbb{L}_i} - \sum_{\mathbb{A}\in\mathcal{V}} f^{\tau_p}_{\mathbb{L}_i,\mathbb{A}} = f_{\mathbb{L}_i^{\tau_p},\mathbb{L}_i^{\tau_{p+1}}} \leqslant W_{\mathbb{L}_i^{\tau_p},\mathbb{L}_i^{\tau_{p+1}}} = C^{\tau_p}_{\mathbb{L}_i}. \tag{8}$$

(d) Observation resource modeling. Due to the satellites movement, multiple observation targets can be in the observation range of same observation satellite. For example, in Figure 7, satellite $\mathbb{O}_1$ has the opportunities to observe both $\mathbb{M}_1$ and $\mathbb{M}_2$ in the third time slot τ_3. However, it is assumed the observation rate of $\mathbb{O}_1$ is limited and total data amount of mission $\mathbb{M}_1$ and $\mathbb{M}_2$ cannot be obtained.

To clearly illustrate, let the maximum observation rate of $\mathbb{O}_i$ be $R_{\mathbb{O}_i}$. Then the maximum amount of data, can be observed by $\mathbb{O}_i$ in τ_p, will be $R_{\mathbb{O}_i} \times |\tau_p|$. And then the constraint introduced by the observation resource for $\mathbb{O}_i$ in τ_p will be

$$\sum_{\mathbb{M}_i\in\mathcal{M}} f^{\tau_p}_{\mathbb{M}_i,\mathbb{O}_i} \leqslant R^{\tau_p}_{\mathbb{O}_i} \times |\tau_p|. \tag{9}$$

To characterize this property of observation resource, which traditional graph cannot model, we design graph representation to split (9) into normal edge constraint and node constraint. For clearness, as shown

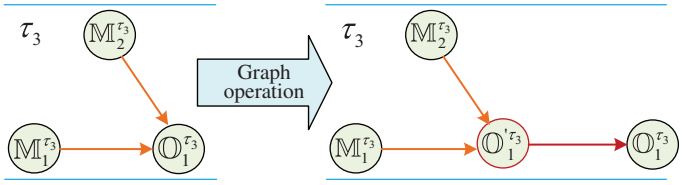

Figure 10 (Color online) Graph operations for observation resource modeling.

in Figure 10, for any observation satellite $\mathbb{O}_1$ in τ_3, virtual node $\mathbb{O}_1'^{\tau_3}$ can be introduced. Then the virtual link $(\mathbb{O}_1'^{\tau_3}, \mathbb{O}_1^{\tau_3})$ can be connected to represent $\mathbb{O}_1$'s observation capacity in τ_3 with $W^{\tau_3}_{\mathbb{O}_1',\mathbb{O}_1} = R^{\tau_3}_{\mathbb{O}_1} \times |\tau_3|$. Moreover, the edges between the mission nodes and $\mathbb{O}_1^{\tau_3}$ should be disconnected while the new edges between the mission nodes and $\mathbb{O}_1'^{\tau_3}$ are connected. And the new edges have the same capacity as their assciated disconnected edges, e.g., $W^{\tau_3}_{\mathbb{M}_2,\mathbb{O}_1'} = W^{\tau_3}_{\mathbb{M}_2,\mathbb{O}_1}$. Note that, the virtual nodes and edges are added in $\mathcal{V}$ and $\mathcal{E}$, respectively, while the disconnected edges are moved out from $\mathcal{E}$.

With the graph operations in Figure 10, the constraint of observation resource is modeled and transformed into flow conservation on node $\mathbb{O}_1'^{\tau_3}$ and link capacity constraints on link $(\mathbb{O}_1'^{\tau_3}, \mathbb{O}_1^{\tau_3})$ as follows:

$$\sum_{\mathbb{M}_i \in \mathcal{M}} f^{\tau_3}_{\mathbb{M}_i,\mathbb{O}_1} = \sum_{\mathbb{M}_i \in \mathcal{M}} f^{\tau_3}_{\mathbb{M}_i,\mathbb{O}_1'} = f^{\tau_3}_{\mathbb{O}_1',\mathbb{O}_1} \leqslant W^{\tau_3}_{\mathbb{O}_1',\mathbb{O}_1} = R^{\tau_3}_{\mathbb{O}_1} \times |\tau_3|. \tag{10}$$

(e) Energy resource modeling. The energy of a satellite is generated by Solar panels and stored in battery cells. Since the Solar panels on satellites are not always oriented to the sun and usually go through the eclipse periods, the energy cannot be continuously generated [25]. Then, the function of battery cells is significant and necessary. However, throughout the whole service life of one battery, only limited charge/discharge times can be conducted. Then, taking full advantage of the available energy is the key to decrease the charge/discharge times and extend the life of batteries. Therefore, it is necessary to accurately model the energy resource.

Let the available energy of the time horizon T for a satellite u be E_u^T. Note that E_u^T is amount of energy that the satellite harvests. Then, let the available energy for data transmission and daily operations of other devices be E_u^- and $E_u^\sim$, respectively. That is,

$$E_u^T = E_u^- + E_u^\sim, \tag{11}$$

where E_u^- depends on the available amount of data that can be transmitted and received by the satellite while $E_u^\sim$ is a constant and independent of the data amount[3)]. Then, our goal is to model E_u^- to make full use of available E_u^- and approach end-to-end transmission performance limits.

As in [26], suppose the bit error rate for the link between satellites (or between satellites and ground stations), is not greater than 10^{-5} and the modulation is BPSK, and then the rate of link is proportional to the transmitter's transmission power. Let the corresponding scale factor for transmitter and receiver be ρ^t and ρ^r, respectively. Let the transmission power and receiving power of node u at time t be $P_u^t(t)$ and $P_u^r(t)$, respectively. Then, we have

$$\begin{aligned} E_u^- &= \int_0^{t_h} [P_u^t(t) + P_u^r(t)]\mathrm{d}t \\ &= \int_0^{t_h} \left[\rho^t \sum_{v\in\mathcal{V}} R_{u,v}(t) + \rho^r \sum_{v\in\mathcal{V}} R_{v,u}(t)\right]\mathrm{d}t \\ &= \rho^t \left[\sum_{v\in\mathcal{V}} \int_0^{t_h} R_{u,v}(t)\mathrm{d}t\right] + \rho^r \left[\sum_{v\in\mathcal{V}} \int_0^{t_h} R_{v,u}(t)\mathrm{d}t\right] \\ &= \rho^t \sum_{v\in\mathcal{V}} \sum_{\tau_p\in T} f^{\tau_p}_{u,v} + \rho^r \sum_{v\in\mathcal{V}} \sum_{\tau_p\in T} f^{\tau_p}_{v,u}. \end{aligned} \tag{12}$$

3) We only focus on the energy consumption and allocation of transceiver resources in this paper, whose energy consumption is considerable. Hence, it is assumed the energy consumption of observation and storage resources are fixed.

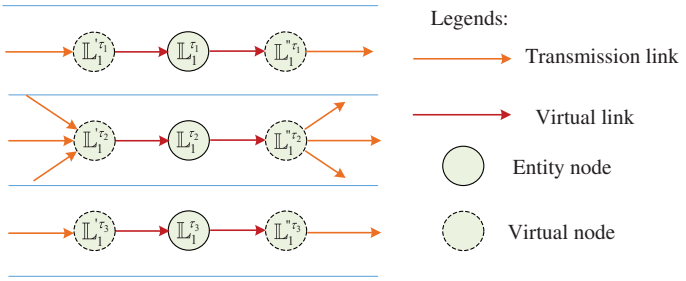

Figure 11 (Color online) Graph operations for energy constraint relation representation.

Hereafter, for end-to-end transmission in SIN, let the source node and destination node be $\mathbb{S}$ and $\mathbb{D}$, respectively. Then, for the node $u \in \mathcal{V}$ other than $\mathbb{S}$ and $\mathbb{D}$, all the received data will be transmitted by the intermediate node throughout T, namely,

$$\sum_{v\in\mathcal{V}}\sum_{\tau_p\in T} f_{u,v}^{\tau_p} = \sum_{v\in\mathcal{V}}\sum_{\tau_p\in T} f_{v,u}^{\tau_p} = \frac{E_u^-}{\rho^t+\rho^r}. \tag{13}$$

And for $\mathbb{S}$ and $\mathbb{D}$, all of $E_{\mathbb{S}}^-$ and $E_{\mathbb{D}}^-$ should be used for transmission and reception, respectively. Naturally, throughout T, the transmitted amount of data of $\mathbb{S}$ equals to the received data of $\mathbb{D}$. Then, we have

$$\sum_{v\in\mathcal{V}}\sum_{\tau_p\in T} f_{\mathbb{S},v}^{\tau_p} = \sum_{v\in\mathcal{V}}\sum_{\tau_p\in T} f_{v,\mathbb{D}}^{\tau_p} = \min\left\{\frac{E_{\mathbb{S}}^-}{\rho^t}, \frac{E_{\mathbb{D}}^-}{\rho^r}\right\}. \tag{14}$$

Eqs. (13) and (14) are brought by the energy resources and are different from (1) and (2), which are difficult to be satisfied . In fact, Eqs. (13) and (14) are similar to the transceiver resource constraints (3) and (4), except that (13) and (14) constrain the data of the whole time horizon T while (3) and (4) constrain only one small time period. Then, given node $\mathbb{L}_1$ in Figure 7, similar representation can be conducted for each time slot as shown in Figure 11.

For the modeling process, graph operations are introduced for each time slot. Specifically, link disconnection and connection operations are conducted, which are the same as that of transceiver modeling. Particularly, the capacity of the $(\mathbb{L}_1', \mathbb{L}_1)$ and $(\mathbb{L}_1, \mathbb{L}_1'')$ for each time slot is set as the available transmission ability (i.e., data amount), namely,

$$W_{\mathbb{L}_1',\mathbb{L}_1}^{\tau_p} = W_{\mathbb{L}_1,\mathbb{L}_1''}^{\tau_p} = \frac{E_u^-}{\rho^t+\rho^r},\ \forall\tau_p\in T,\ \mathbb{L}_1\in\mathcal{V}-\{s,d\}. \tag{15}$$

For $\mathbb{S}$ and $\mathbb{D}$, only the virtual 'transmission link' $(\mathbb{S}, \mathbb{S}'')$ is inserted for $\mathbb{S}$ in each time slot. And then the links connected with $\mathbb{S}$ in each time slot are disconnected. Next, $\mathbb{S}''$ will be linked to the nodes which are used to connect with $\mathbb{S}$. In particular, the new links have the same capacity as the associated disconnected links (e.g., $W_{\mathbb{S}'',u}^{\tau_p} = W_{\mathbb{S},u}^{\tau_p}$). Meanwhile, the virtual 'reception link' $(\mathbb{D}', \mathbb{D})$ is inserted for destination node $\mathbb{D}$ in each time slot, similar link connection and disconnection operations will be conducted. Specially, the capacity of virtual links are assigned as follows:

$$W_{\mathbb{S},\mathbb{S}''}^{\tau_p} = W_{\mathbb{D}',\mathbb{D}}^{\tau_p} = \min\left\{\frac{E_{\mathbb{S}}^-}{\rho^t}, \frac{E_{\mathbb{D}}^-}{\rho^r}\right\},\ \forall\tau_p\in T. \tag{16}$$

Note that, to avoid pre-allocation of energy resource, we label the available energy throughout T on the link of each time slot. Unfortunately, given any node $\mathbb{L}_1$, with the representation, only part of (13) and (14) can be transformed into flow conservation constraints on $\mathbb{L}_1'$, $\mathbb{L}_1''$ and capacity constraints on $(\mathbb{L}_1', \mathbb{L}_1)$ and $(\mathbb{L}_1, \mathbb{L}_1'')$. Special computation rules are needed to jointly schedule the energy, caching and transceiver resources, which is illustrated in Section 4.

(f) Characteristics and applications of ETEG. As a result, resorting to Figure 12, ETEG jointly models the caching, observation, energy, and transceiver resources for SIN in Figure 6. Then, to complete mission $\mathbb{M}_1$ and $\mathbb{M}_2$, path $(\mathbb{M}_1^{\tau_1}, \mathbb{O}_1'^{\tau_1}, \mathbb{O}_1^{\tau_1}, \mathbb{O}_1^{\tau_2}, \mathbb{O}_1''^{\tau_2}, \mathbb{L}_1'^{\tau_2}, \mathbb{L}_1^{\tau_2}, \mathbb{L}_1''^{\tau_2}, \mathbb{L}_2'^{\tau_2}, \mathbb{L}_2^{\tau_2}, \mathbb{L}_2^{\tau_3}, \mathbb{L}_2''^{\tau_3}, \mathbb{G}'^{\tau_3}, \mathbb{G}^{\tau_3})$ and $(\mathbb{M}_2^{\tau_2}, \mathbb{O}_1'^{\tau_2}, \mathbb{O}_1^{\tau_2}, \mathbb{O}_1''^{\tau_2}, \mathbb{L}_1'^{\tau_2}, \mathbb{L}_1^{\tau_2}, \mathbb{L}_1''^{\tau_2}, \mathbb{L}_2'^{\tau_2}, \mathbb{L}_2^{\tau_2}, \mathbb{L}_2^{\tau_3}, \mathbb{L}_2''^{\tau_3}, \mathbb{G}'^{\tau_3}, \mathbb{G}^{\tau_3})$ can be identified in ETEG, respectively. While in snapshot graph Figure 7, no paths can be found from mission nodes to ground stations

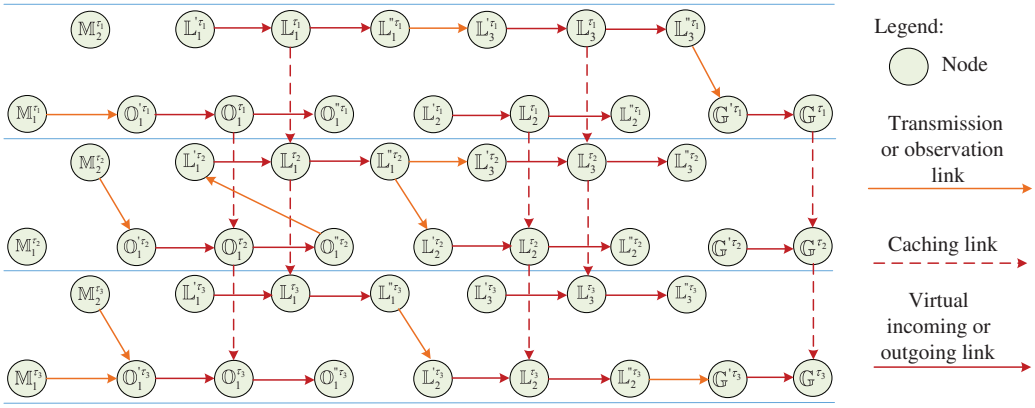

Figure 12 (Color online) ETEG based modeling for SIN in Figure 6.

Table 1 Representation ability of different graphs

Resource elements	Whether traditional graph can model	Whether TEG can model	Whether ETEG can model
Static topology	YES	YES	YES
Time-varying topology	NO	YES	YES
Caching resource	NO	YES	YES
Observation resource	NO	NO	YES
Transceiver resource	NO	NO	YES
Energy resource	NO	NO	YES

nodes. Note that, two kinds of weights coexist for some links (e.g., $(\mathbb{L}_1^{\prime\tau_2}, \mathbb{L}_1^{\tau_2})$), where one weight is for transceiver and another is for energy weight. To distinguish the two weights, let the transceiver and energy resource weight be TW and EW, respectively.

We consider a satellite network with n nodes and m edges in one time slot and the time horizon T are split into h time slots, then time-expanded graph will have hn nodes and $hm + (h-1)n$ edges. For our ETEG, we introduce two extra virtual nodes for each satellite nodes, then ETEG has at most $3hn$ nodes. Similarly, ETEG add two virtual links for each nodes and has $hm+3hn$ edges. Note that in worst case, $m = n(n-1) \gg 3n$, therefore, our proposed ETEG will not effect the computation and storage complexity in essence compared with TEG.

As shown in Table 1, we show the modeling ability of traditional graph, TEG, and our proposed ETEG. From the table, we can see that our proposed ETEG jointly model the multi-dimensional resources, which support joint scheduling of the multiple resources to maximize network profit. In particular, other resources in different areas (e.g., cargo delivery, product processing) possessing similar constraints can adopt our proposed modeling method.

4 ETEG-based resource scheduling algorithm

In fact, a graph-based maximum flow algorithm enables to make optimal utilization of network resources such that the maximum network capacity from the source node to the destination node can be achieved. Fortunately, our ETEG jointly represents the heterogeneous caching, observation, transceiver, and energy resources as uniform links in ETEG, and quantifies the different types of resources as link weights. Therefore, through ETEG, the problem, joint scheduling of caching, observation, transceiver and energy resources to maximize the data volume of observation missions obtained by ground stations, can be transformed into a maximum flow one, whereby all mission nodes and ground station nodes can be viewed as source and destination nodes, respectively.

Given ETEG $= \{T, \mathcal{V}, \mathcal{E}, W, f\}$, our goal is to determine $f_{u,v}$ for each link $(u, v) \in \mathcal{E}$ so that the data amount of observed missions that have been successfully transmitted to the ground, can be maximized. Specially, caching or observation links only have weight W to indicate the caching space or observation capacity. The transceiver and energy representation share the same links. Thus, these links have two kinds of weights, TW and EW, to depict the links' available transceiver and energy capacity, respectively. Hence, let edge set $\mathcal{E}_s \subset \mathcal{E}$ be the special collection of the energy and transceiver links. Furthermore, path

from source s to destination d is defined as $P = \{(s,u),(u,v),\ldots,(p,d)\}$, which is a set of subsequent links. As such, we modify the traditional Edmonds-Karp maximum flow algorithm as in Algorithm 1.

Algorithm 1 Enhanced-time expanded graph based maximum flow algorithm

Input: Residual network rETEG = ETEG $= \{T, \mathcal{V}, \mathcal{E}, W, f\}$, mission nodes set $\mathcal{M}$ and the special edge set $\mathcal{E}_s \subset \mathcal{E}$.
while feasible paths exist from missions to ground stations in rETEG **do**
  update the links' weight of $\mathcal{E}_s$ through $W^{\tau_p}_{u,v} = \min\{\mathrm{TW}^{\tau_p}_{u,v}, \mathrm{EW}^{\tau_p}_{u,v}\}$;
  identify a feasible path P using breadth-first search (BFS) algorithm [24], so that for $\forall(u^{\tau_p}, v^{\tau_p}) \in P$, $W^{\tau_p}_{u,v} > 0$;
  compute the maximum feasible flow value $F(P)$ of path P, and $F(P) = \min\{W^{\tau_p}_{u,v} | (u^{\tau_p}, v^{\tau_p}) \in P\}$;
  for each edge $(u^{\tau_p}, v^{\tau_p}) \in P$ **do**
    if $(u^{\tau_p}, v^{\tau_p}) \in \mathcal{E}_s$ **then**
      $\mathrm{TW}^{\tau_p}_{u,v} \leftarrow \mathrm{TW}^{\tau_p}_{u,v} - F(P)$; $\mathrm{TW}^{\tau_p}_{v,u} \leftarrow \mathrm{TW}^{\tau_p}_{v,u} + F(P)$;
      for $\tau_p \in T$ **do**
        $\mathrm{EW}^{\tau_p}_{u,v} \leftarrow \mathrm{EW}^{\tau_p}_{u,v} - F(P)$; $\mathrm{EW}^{\tau_p}_{v,u} \leftarrow \mathrm{EW}^{\tau_p}_{v,u} + F(P)$;
      end for
    else
      $W^{\tau_p}_{u,v} \leftarrow W^{\tau_p}_{u,v} - F(P)$; $W^{\tau_p}_{v,u} \leftarrow W^{\tau_p}_{v,u} - F(P)$;
    end if
  end for
end while

The main idea of this algorithm can be divided into 3 steps. The first step is to find feasible paths from source to destination nodes with a nonnegative flow. Next, for each found path, its feasible flow is the minimum link weight of all links along the path. Note that, for the energy and transceiver representation link, its available weight is the minimum of TW and EW. Finally, the residual network is updated based on the path. Note that, for each energy link along the path, not only does the link's EW need to be updated, but also the corresponding links' EWs need to be updated. That is, if a satellite $\mathbb{L}_i$ consumes some energy in $\tau_p \in T$, then the available energy of $\mathbb{L}_i$ for all the other time slots $\tau_q \in T$, $q \neq p$ should be changed as all these links share the energy $E^-_{\mathbb{L}_i}$.

Particularly, the maximum flow result reflects on resource scheduling decisions. For the identified path P with a feasible flow value $F(P)$, suppose it includes caching link $(\mathbb{L}_i^{\tau_p}, \mathbb{L}_i^{\tau_{p+1}})$, observation link $(\mathbb{M}_i, \mathbb{O}_j^{\tau_p})$, transmission link $(\mathbb{L}_m^{\prime\prime\tau_p}, \mathbb{L}_n^{\prime\tau_p})$, and energy and transceiver link $(\mathbb{L}_i^{\prime\tau_p}, \mathbb{L}_i^{\tau_p})$. The flow across different links indicates different resource scheduling decisions. For instance, $(\mathbb{L}_i^{\tau_p}, \mathbb{L}_i^{\tau_{p+1}})$ indicates that satellite $\mathbb{L}_i$ will store $F(P)$ amount data from τ_p to τ_{p+1}, while $(\mathbb{M}_i, \mathbb{O}_j^{\tau_p})$ implies $\mathbb{O}_j$ will use its camera to observe mission $\mathbb{M}_i$ in τ_p. Besides, $(\mathbb{L}_m^{\prime\prime\tau_p}, \mathbb{L}_n^{\prime\tau_p})$ represents $\mathbb{L}_m$ will consume energy and transmitter resources to transmit $F(P)$ data to $\mathbb{L}_n$ in τ_p, while $\mathbb{L}_n$ also consumes energy and receiver resources to receive $F(P)$ data. Finally, $(\mathbb{L}_i^{\prime\tau_p}, \mathbb{L}_i^{\tau_p})$ represents the amount of data, that $\mathbb{L}_i$'s remaining energy and receiver resources can support to receive, is decreased by $F(P)$. Similarly, the transmission energy and transmitter resources of $\mathbb{L}_i$ will be scheduled in τ_p if flow goes across $(\mathbb{L}_i^{\tau_p}, \mathbb{L}_i^{\prime\prime\tau_p})$.

In fact, it is the ground stations that accept observation requests and make the scheduling decisions. Then, the scheduling decisions can be uploaded to the satellites as instructions through the ground measurement and control network for satellite networks. Since all the scheduling decisions are made on the ground and the state of the available resources for each satellite in the time horizon T are known, the ground can always schedule resources with the network information.

5 Simulation

A satellite network is considered for simulations, which contains 4 observation satellites at heights of 962 km with inclination of 82.9° and 5 LEO relay satellites randomly selected from the Iridium constellation. Besides, Sanya (18°N, 109.5°E) and Kashi (39.5°N, 76°E) are chosen as the locations of 2 ground stations, respectively. Furthermore, 200 observation missions are randomly selected from earth surface with latitude from 30°S to 30°N and longitude from 10°E and 70°E, and the mission data volume randomly takes a value from {4,6,8} Gb. Besides, each satellite is equipped with two transceivers, and each transceiver provides a maximum transmission and reception rate, randomly chosen from {20, 25, 30} Mbps. Moreover, the observation rate is set as 40 Mbps, and the caching space of each satellite is 100 GB. Furthermore, it is assumed the available energy E^-_u for communication of each satellite is 150 kJ in $T = 6$ h, which will not violate the capacity of battery cells (i.e., 5000 Watt Minute) as in [25]. Then, referring to [26], each satellite's energy factors for transmission and reception are $\rho^t = 0.05$ Watt/Mbps

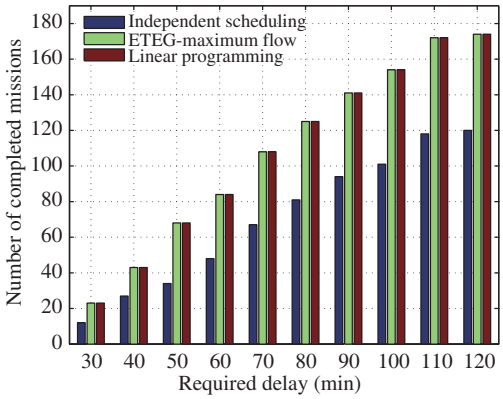

Figure 13 (Color online) The number of completed missions with different delay requirements of missions.

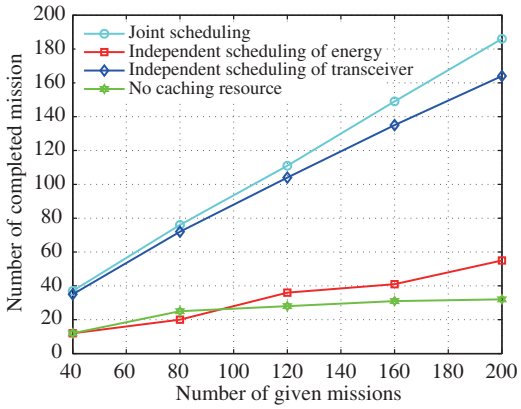

Figure 14 (Color online) The number of completed missions given different missions.

Table 2 Running time (s) of the MILP, LP, and ETEG-based method

Method	$T = 4$ h	$T = 8$ h	$T = 12$ h	$T = 16$ h	$T = 20$ h
ETEG	0.06	0.14	0.23	0.4	0.77
LP	8	18.3	247	520	858
MILP	23.5	127.9	82038	–	–

$= 0.05$ J/Mb and $\rho^r = 0.01$ Watt/Mbps $= 0.01$ J/Mb, respectively.

To demonstrate the performance, the earth observation and transmission missions scheduling problem is considered. The objective is to maximize the number of observed missions which have been successfully transmitted to the ground, while the caching, observation, transceiver, and energy resource constraints should be satisfied.

First, our maximum flow-based joint scheduling is compared to optimal linear programming and independent observation and transmission scheduling, as shown in Figure 13. The scheduling time horizon $T = 6$ h and the delay requirements of missions vary from 30 to 120 min with 10 min step size. Note that, the linear programming is solved by the OSQP solver belonging to CVXPY [27], while the observation and transmission scheduling of the independent scheduling scheme are optimally solved using maximum flow algorithm [21] and QoS support strategy [16], respectively. The result shows the optimality of our algorithm, since it met the same number of missions as LP. Besides, our joint-scheduling method outperforms independent scheduling since it identifies paths containing both observation and subsequent transmission, and the independent scheduling could cause mismatch between observation and transmission. Furthermore, all the schemes can complete more missions as the delay requirements increase, since more resources can be used. Particularly, we compare the running time of our ETEG-based maximum flow to those of LP and MILP [7] models, with time horizon T ranging from 4 to 20 h. And the MILP is solved by GUROBI solver. As shown in Table 2, while finishing the same number of missions, our ETEG-based method is still distinguished in terms of computational speed. And when T reaches 16 and 20 h, the result for the MILP model is untractable.

Then to show the importance of cooperation of the resources and nodes, we compare the ETEG-based scheme with other 3 schemes in Figure 14. They are (1) maximum flow algorithm with energy resources randomly allocated in each time slot, (2) maximum flow algorithm with transceiver resources randomly allocated and (3) maximum flow algorithm without caching resource involved. The trend that more missions are completed when more missions are inserted into the network is expected, which can be explained by that more resources are utilized when more missions are added. Furthermore, we can see that without cooperation of multiple resources and nodes, independent allocation of energy and transceiver resources will lead to poor performance. Besides, without caching resource involved, only a little number of missions can be completed, which shows the importance of caching resource in SIN.

6 Conclusion

In this paper, we jointly characterize the observation, caching, transceiver, and energy resources for SIN by introducing virtual links and nodes and construct the enhanced time expanded graph. Then the graph's advantage of low complexity can be made full use of and SIN can obtain better performance with resource cooperation. In the future, we will focus on the graph modeling of the robustness for SIN.

Acknowledgements This work was supported by National Natural Science Foundation of China (Grant No. 61871456).

References

1 Sheng M, Zhou D, Liu R Z, et al. Resource mobility in space information networks: opportunities, challenges, and approaches. IEEE Netw, 2019, 33: 128–135
2 Du J, Jiang C X, Guo Q, et al. Cooperative earth observation through complex space information networks. IEEE Wirel Commun, 2016, 23: 136–144
3 Zhang T, Li J D, Li H Y, et al. Application of time-varying graph theory over the space information networks. IEEE Netw, 2020, 34: 179–185
4 Jiang C X, Wang X X, Wang J, et al. Security in space information networks. IEEE Commun Mag, 2015, 53: 82–88
5 Fortz B, Rexford J, Thorup M. Traffic engineering with traditional IP routing protocols. IEEE Commun Mag, 2002, 40: 118–124
6 Guerin R A, Orda A, Williams D. QoS routing mechanisms and OSPF extensions. In: Proceedings of IEEE Global Telecommunications Conference, Phoenix, 1997. 1903–1908
7 Liu R Z, Sheng M, Lui K S, et al. An analytical framework for resource-limited small satellite networks. IEEE Commun Lett, 2016, 20: 388–391
8 Zhou D, Sheng M, Wang X J, et al. Mission aware contact plan design in resource-limited small satellite networks. IEEE Trans Commun, 2017, 65: 2451–2466
9 Wang Y, Sheng M, Zhuang W H, et al. Multi-resource coordinate scheduling for earth observation in space information networks. IEEE J Sel Areas Commun, 2018, 36: 268–279
10 Huang J H, Su Y X, Huang L, et al. An optimized snapshot division strategy for satellite network in GNSS. IEEE Commun Lett, 2016, 20: 2406–2409
11 Shi K Y, Zhang X S, Zhang S, et al. Time-expanded graph based energy-efficient delay-bounded multicast over satellite networks. IEEE Trans Veh Technol, 2020, 69: 10380–10384
12 Wang P, Zhang X S, Zhang S, et al. Time-expanded graph-based resource allocation over the satellite networks. IEEE Wirel Commun Lett, 2019, 8: 360–363
13 Jiang C X, Zhu X M. Reinforcement learning based capacity management in multi-layer satellite networks. IEEE Trans Wirel Commun, 2020, 19: 4685–4699
14 George B, Shekhar S. Time-aggregated graphs for modeling spatio-temporal networks. In: Proceedings of Time-Aggregated Graphs for Modeling Spatio-Temporal Networks, 2006. 85–99
15 Li H Y, Zhang T, Zhang Y K, et al. A maximum flow algorithm based on storage time aggregated graph for delay-tolerant networks. Ad Hoc Netw, 2017, 59: 63–70
16 Zhang T, Li H Y, Zhang S, et al. STAG-based QoS support routing strategy for multiple missions over the satellite networks. IEEE Trans Commun, 2019, 67: 6912–6924
17 Zhang T, Li H Y, Li J D, et al. A dynamic combined flow algorithm for the two-commodity max-flow problem over delay-tolerant networks. IEEE Trans Wirel Commun, 2018, 17: 7879–7893
18 Zhang Z Q, Jiang C X, Guo S, et al. Temporal centrality-balanced traffic management for space satellite networks. IEEE Trans Veh Technol, 2018, 67: 4427–4439
19 Goldberg A V, Tarjan R E. Efficient maximum flow algorithms. Commun ACM, 2014, 57: 82–89
20 Li P Y, Li J D, Li H Y, et al. Graph based task scheduling algorithm for earth observation satellites. In: Proceedings of IEEE Global Communications Conference, Abu Dhabi, 2018
21 Ravindra K A, Thomas L M, James B O, Network flows — theory, algorithms and applications. J Oper Res Soc, 1993, 45: 791–796
22 Chen X J, Wan J X. Development status and proposals for multi-beam antennas of communication satellites. Space Elect Technol, 2016, 2: 54–60
23 Ren J Q, Zhou H G, Zhou N, et al. Application of phased array anttena and fixed multibeam antennna in communications satellite systems. Space Int, 2015, 11: 55–60
24 Ford L R J, Fulkerson D R. Constructing maximal dynamic flows from static flows. Oper Res, 1958, 6: 419–433
25 Yang Y, Xu M W, Wang D, et al. Towards energy-efficient routing in satellite networks. IEEE J Sel Areas Commun, 2016, 34: 3869–3886
26 Tian Y R, Lu X C, Huang F J. Design and performance analysis of inter-satellite link in multilayer satellite network (in Chinese). J Time Freq, 2010, 33: 140–145
27 Diamond S, Boyd S. CVXPY: a python-embedded modeling language for convex optimization. J of Machi Lear Res, 2016, 17: 1–5